

Proton temperature-anisotropy-driven instabilities in weakly collisional plasmas: Hybrid simulations

Petr Hellinger^{1,2} and Pavel M. Trávníček^{3,1,2}

¹Astronomical Institute AS CR, Bocni II/1401, CZ-14131 Prague, Czech Republic

²Institute of Atmospheric Physics, AS CR, Bocni II/1401, CZ-14131 Prague, Czech Republic

³Space Sciences Laboratory, UCB, Berkeley, USA.

(Received ?; revised ?; accepted ?.)

Kinetic instabilities in weakly collisional, high beta plasmas are investigated using two-dimensional hybrid expanding box simulations with Coulomb collisions modeled through the Langevin equation (corresponding to the Fokker-Planck one). The expansion drives a parallel or perpendicular temperature anisotropy (depending on the orientation of the ambient magnetic field). For the chosen parameters the Coulomb collisions are important with respect to the driver but are not strong enough to keep the system stable with respect to instabilities driven by the proton temperature anisotropy. In the case of the parallel temperature anisotropy the dominant oblique fire hose instability efficiently reduces the anisotropy in a quasilinear manner. In the case of the perpendicular temperature anisotropy the dominant mirror instability generates coherent compressive structures which scatter protons and reduce the temperature anisotropy. For both the cases the instabilities generate temporarily enough wave energy so that the corresponding (anomalous) transport coefficients dominate over the collisional ones and their properties are similar to those in collisionless plasmas.

1. Introduction

Large scale (turbulent) motion of the plasma often leads to changes in the magnitude of the magnetic field (and possibly also in the particle densities). Such changes tend to generate particle temperature anisotropies. In collisionless plasmas where no important wave activity or heat fluxes are present the two first adiabatic invariants are expected to be conserved and, consequently, the parallel and perpendicular temperatures (with respect to the ambient magnetic field) behave differently (Chew *et al.* 1956). Coulomb collisions naturally reduce the temperature anisotropies but may not be sufficient to keep the plasma in thermal equilibrium. The plasma system may eventually become unstable with respect to temperature-anisotropy driven instabilities. For example, in the case of the almost collisionless solar wind plasmas protons exhibit relatively large temperature anisotropies with signatures of bounds imposed by kinetic instabilities (Hellinger *et al.* 2006; Wicks *et al.* 2013; Bale *et al.* 2009; Hellinger & Trávníček 2014). Similar effects are expected in other astrophysical situations such as in the intercluster high-beta plasmas (Rosin *et al.* 2011; Santos-Lima *et al.* 2014) where Coulomb collisions are expected to play an important role but where even a very weak temperature anisotropy may drive the system unstable.

Coulomb collisions and kinetic instabilities are relatively well understood as separate processes. The collective behavior of the Coulomb collisions is usually studied in the approximation of two-particle interactions which leads to the Boltzmann integral equation.

This equation may be further approximated by considering only small-angle scattering events; this leads to a differential Fokker-Planck equation which considerably simplifies the modeling of Coulomb collisions. However, it is important to keep in mind that the Fokker-Planck approximation is not generally applicable (with respect to the Boltzmann integral approximation) even for Maxwellian particle velocity distribution functions (Shoub 1987). Coulomb collisions have a kinetic nature. The scattering cross section is strongly dependent on the relative particle velocity and a collisionality in different regions of the velocity distribution function varies significantly.

Kinetic instabilities in plasmas are typically studied in homogeneous collisionless plasmas. The linear properties of these instabilities are generally described by a complicated system which needs to be treated numerically except in some limiting cases. Kinetic instabilities tend to reduce the source of free energy but their nonlinear properties are not fully understood. Assuming a superposition of weak/noninteracting random phase modes leads to a quasi-linear approximation with a diffusion in the velocity space owing to averaged second order terms (Kennel & Engelmann 1966; Hellinger & Trávníček 2012). Presence of important wave-wave interactions, wave coherence or of an important population of trapped particles, however, makes this approach questionable.

Sufficiently strong Coulomb collisions invalidate the collisionless approach. Particle trajectories are modified by collisions so that wave-particle interactions and particle trapping are likely importantly influenced by the strong collisions. The collisions typically introduce a damping so that one expects that they increase instability thresholds or even suppress instabilities. On the other hand, wave-particle interactions often lead to formation of small-scale structures in the particle velocity distribution functions. Large gradients connected with such structures would lead to an enhanced collisional diffusion in the Fokker-Planck approach (cf., Schekochihin *et al.* 2008). However, the Fokker-Planck equation is only an approximation of an approximation of another approximation. From the more general Boltzmann integral approach it is not clear that strong gradients in the particle velocity distribution functions importantly affect the collisional interaction.

The situation becomes more complicated when there is an external driver which generates the temperature anisotropy. The system behavior depends on relative time scales of the three process. However, both Coulomb collisions and instabilities are kinetic so that their characteristic times are different in different regions of the particle velocity distribution function. For collisions one can define an average macroscopic time scale but in the case of instabilities it is more complicated. One possible measure of the instability time scale is the (maximum) growth rate which typically increases monotonically above threshold. Hybrid collisionless simulations with external drivers (expansion, velocity shears) indicate that as the system enters the unstable regions waves are generated. When these waves have strong enough amplitude they are able to some extent counteract the driven anisotropization and to keep the system near the marginal stability (Hellinger & Trávníček 2005; Matteini *et al.* 2006; Kunz *et al.* 2014). This evolution depends on the time scale of the driver. In the driven simulations the system enters further to the unstable region and generates stronger wave activity for a faster driver. This process can be to some extent modeled by a bounded anisotropy model (Denton *et al.* 1994; Hellinger & Trávníček 2008; Chandran *et al.* 2011) where the linear prediction is used to impose bounds on the temperature anisotropy by introducing a strong effective isotropization frequency in the unstable region.

The feedback of Coulomb collisions and kinetic instabilities on the large scale driver is another open problem. The effects of the Coulomb collisions on the macroscopic level may be expressed by transport coefficients which are typically derived in the vicinity of thermal equilibrium (Braginskii 1965). A presence of other kinetic effects may render

questionable these collision-dominated theoretical predictions (in the collisionless limit the transport coefficients of Braginskii (1965) diverge). Some collisional transport coefficients can be calculated even far from thermal equilibrium, for example assuming drifting bi-Maxwellian velocity distribution functions for all particle species (Barakat & Schunk 1981; Hellinger & Trávníček 2009). For instance the proton-proton isotropization frequency ν_{pp}

$$\left[\frac{d(T_{p\perp} - T_{p\parallel})}{dt} \right]_{\text{coll}} = -\nu_{pp} (T_{p\perp} - T_{p\parallel}) \quad (1.1)$$

may be given as

$$\nu_{pp} = \frac{e^4 n_p \ln \Lambda}{10\pi^{3/2} \epsilon_0^2 m_p^{1/2} k_B^{3/2} T_{p\parallel}^{3/2}} {}_2F_1 \left(\begin{matrix} 2, 3/2 \\ 7/2 \end{matrix}, 1 - \frac{T_{p\perp}}{T_{p\parallel}} \right) \quad (1.2)$$

where ${}_2F_1$ is the standard (Gauss) hypergeometric function. In collisionless plasmas kinetic instabilities lead to effective transport coefficients. In the quasi-linear approximation it is possible to derive some of the transport coefficients (Yoon & Seough 2012; Hellinger *et al.* 2013) assuming the particle velocity distribution function is close to bi-Maxwellian.

The behavior of a driven system with Coulomb collisions and temperature anisotropy-driven instabilities is a complex nonlinear problem which is hard to investigate analytically so that a numerical approach is needed. In this paper we investigate expansion driven proton temperature anisotropies in high beta, weakly collisional plasmas. In high beta (collisionless) plasmas there are two dominant instabilities driven by the proton temperature anisotropy. For $T_{p\perp} > T_{p\parallel}$ it is the mirror instability (Hasegawa 1969). This instability is resonant (i.e., a substantial portion of the proton velocity distribution function resonates with the unstable waves (cf., Gary 1993)) through the Landau resonance. This kinetic feature is combined with fluid properties, the unstable waves are nonpropagating and have long wavelengths near threshold. The nonlinear properties of the mirror instability are not fully understood, as they seem to combine kinetic properties (the Landau resonance, particle scattering/trapping) and a fluid nonlinearity (Califano *et al.* 2008). For $T_{p\perp} < T_{p\parallel}$ the dominant growing mode is the oblique fire hose instability (Hellinger & Matsumoto 2000). This instability is resonant through the cyclotron resonance and generates transient nonpropagating modes which eventually become propagating and damped (Hellinger & Trávníček 2008). Other instabilities (ion cyclotron, parallel fire hose, Weibel) may also play an important role in regulating the proton temperature anisotropy.

This paper is organized as follows: section 2 describes the numerical code, section 3 presents the simulation results for one simulation for the parallel proton temperature anisotropy $T_{p\perp} < T_{p\parallel}$ and one for the perpendicular anisotropy $T_{p\perp} > T_{p\parallel}$. The simulation results are summarized and discussed in section 4.

2. Expanding box model

Here we use the expanding box model (Grappin *et al.* 1993) implemented to the hybrid code developed by Matthews (1994) to study a response of a weakly collisional plasma to a slow expansion. In this Collisional Hybrid Expanding Box (CHEB) model the expansion is described as an external force. This model was developed in the context of the radial expansion of the solar wind. One assumes a solar wind with a constant radial velocity U at a radial distance R . Transverse scales (with respect to the radial direction) of a small portion of plasma, co-moving with the solar wind velocity, increase with time as $1 + t/t_e$

where $t_e = R_0/U$ is the (initial) characteristic expansion time. The expanding box uses these co-moving coordinates, the physical transverse scales of the simulation box increase with time (see Hellinger & Trávníček 2005, for a detailed description of the (collisionless) code) and the standard periodic boundary conditions are used. Coulomb collisions in the code are modelled using the Langevin stochastic forcing corresponding to the Fokker-Planck equation (Manheimer *et al.* 1997) where particle velocity distribution functions are assumed to be drifting bi-Maxwellian ones; in this case Rosenbluth potentials can be expressed in terms of generalized triple hypergeometric functions and the corresponding Langevin stochastic equation can be constructed (cf., Hellinger & Trávníček 2010).

The characteristic spatial and temporal units used in the model are the initial proton inertial length $d_{p0} = c/\omega_{pp0}$ and the inverse initial proton cyclotron frequency $1/\omega_{cp0}$. Here c is the speed of light, $\omega_{pp0} = (n_{p0}e^2/m_p\epsilon_0)^{1/2}$ is the initial proton plasma frequency, $\omega_{cp0} = eB_0/m_p$, B_0 is the initial magnitude of the ambient magnetic field \mathbf{B}_0 , n_{p0} is the initial proton density, e and m_p are the proton electric charge and mass, respectively; finally, ϵ_0 is the dielectric permittivity of vacuum. We use the spatial resolution $\Delta x = \Delta y = 2c/\omega_{pp0}$, and there are initially 16.384 particles per cell for protons. Fields and moments are defined on a 2-D grid 512×512 . Protons are advanced using the Boris' scheme with a time step $\Delta t = 0.05/\omega_{cp0}$, while the magnetic field \mathbf{B} is advanced with a smaller time step $\Delta t_B = \Delta t/10$. The collisional Langevin stochastic forcing is applied every 10 time steps. The initial ambient magnetic field is directed along x direction, $\mathbf{B}_0 = (B_0, 0, 0)$.

We analyze two simulations, one for the parallel proton temperature anisotropy $T_{p\perp} < T_{p\parallel}$ and one for the perpendicular anisotropy $T_{p\perp} > T_{p\parallel}$. We assume relatively high proton betas (~ 20) and relatively high Coulomb collisional rates (with respect to the expansion time). These parameters are quite larger than those typically observed in the solar wind as here we are more interested in high-beta astrophysical plasmas (such as the intercluster plasmas where, however, even much larger plasma betas are expected).

3. Simulation results

3.1. Fire hose instabilities

In the first (fire hose), 2-D CHEB simulation we initialize protons as an isotropic Maxwellian velocity distribution function with $\beta_p = 20$. We impose a continuous expansion in the y and z directions (transverse with respect to the ambient magnetic field) with the (initial) characteristic expansion time $t_e = 10^4/\omega_{cp0}$. The proton density and the magnitude of the ambient magnetic field decrease as $(1 + t/t_e)^{-2}$ due to the expansion. Such a decrease would lead in a collisionless plasma to the double adiabatic evolution when no wave activity or heat fluxes are present (Chew *et al.* 1956):

$$\left(\frac{dT_{p\perp}}{dt}\right)_{\text{CGL}} = \frac{T_{p\perp}}{B} \frac{dB}{dt} \quad \text{and} \quad \left(\frac{dT_{p\parallel}}{dt}\right)_{\text{CGL}} = 2\frac{T_{p\parallel}}{n} \frac{dB}{dt} - 2\frac{T_{p\parallel}}{B} \frac{dB}{dt}; \quad (3.1)$$

in this case $T_{p\perp}/T_{p\parallel}$ would decrease with time. For the Coulomb collision we set the initial isotropization frequency $\nu_{pp} = 1.2 \times 10^{-3}\omega_{cp}$. The expanding collisional system is expected to follow an evolution where double-adiabatically driven development of the temperature anisotropy is counteracted by Coulomb collisions (when no wave activity or heat fluxes are present)

$$\frac{dT_{p\perp,\parallel}}{dt} = \left(\frac{dT_{p\perp,\parallel}}{dt}\right)_{\text{CGL}} + \left(\frac{dT_{p\perp,\parallel}}{dt}\right)_{\text{coll}} \quad (3.2)$$

where

$$\left(\frac{dT_{p\perp}}{dt}\right)_{\text{coll}} = -\frac{1}{2}\left(\frac{dT_{p\parallel}}{dt}\right)_{\text{coll}} = -\frac{\nu_{pp}}{3}(T_{p\perp} - T_{p\parallel}). \quad (3.3)$$

and where ν_{pp} is given by Equation (1.2) when the proton velocity distribution functions are close to bi-Maxwellian ones

The evolution in the expanding system is shown in Figure 1 in the $(\beta_{p\parallel}, T_{p\perp}/T_{p\parallel})$ space. The solid curves denote the path in the 2-D (fire hose) CHEB simulation where $\beta_{p\parallel}$ and $T_{p\perp}/T_{p\parallel}$ are averaged quantities over the simulation box calculated with respect to the ambient magnetic field. The dashed contours show the linear (collisionless) prediction, the maximum linear growth rate (in units of ω_{cp}) as a function of $\beta_{p\parallel}$ and $T_{p\perp}/T_{p\parallel}$ for the oblique fire hose (left panel) and for the parallel fire hose (right panel). The dotted line on the left panel shows the theoretical collisional evolution (obtained from Eq. (3.2)) whereas the dash-dotted line displays the fluid fire hose threshold $C_F = 0$ where

$$C_F = \beta_{\parallel} - \beta_{\perp} - 2. \quad (3.4)$$

Figure 1 shows that initially the system follows the theoretical prediction of Eq. (3.2); $T_{p\perp}/T_{p\parallel}$ decreases as the Coulomb collisions are not strong enough to keep the protons isotropic. The initial behavior of the system is almost double adiabatic as the collisional isotropization is proportional to $|T_{p\perp} - T_{p\parallel}|$. As the temperature anisotropy grows the system departs from the double adiabatic expectation, and, eventually, the collisional term would dominate and the system would asymptotically reach the isotropy. Note that the expansion driving decreases with time (as the expansion time R/U increases). In the simulation, however, the system becomes unstable with respect to the oblique fire hose before the collisions become dominant and the proton temperature anisotropy is strongly reduced. After this $T_{p\perp}/T_{p\parallel}$ decreases again and this evolution periodically repeats itself. In the 2-D (fire hose) CHEB the system is linearly stable with respect to the proton parallel fire hose which has a higher threshold close to the fluid one.†

To test the relevance of the (collisionless) quasi-linear approximation for the description of the oblique fire hose we have developed a simple, one-mode quasi-linear model for the instability as a more physical version of a bounded anisotropy model. In this model only one mode is considered and is assumed to have the growth-rate and quasi-linear diffusion properties of the most unstable mode. In the stable region the amplitude of this mode is assumed to be constant (the mode starts with a small, dynamically negligible amplitude) and no diffusion is assumed whereas in the (collisionless) unstable region this mode grows following the (collisionless) prediction based on bi-Maxwellian VDFs $d\delta B/dt = \gamma_{max}\delta B$ (changes in the position of the most unstable mode in the wave vector space are ignored); the quasi-linear heating rates $(dT_{p\perp,\parallel}/dt)_{QL}$ are calculated for the most unstable mode also assuming bi-Maxwellian VDFs (Hellinger *et al.* 2013). The result of this model is shown on Figure 1 (right panel, dotted line). The simple model captures relatively well the initial excursion of the system to the unstable region and after the saturation, it predicts a marginal stability path with respect to the oblique fire hose instability.

The evolution of the wave spectrum in the simulation is shown in Figure 2. Figure 2 (top panel) displays the fluctuating magnetic field $\delta B^2/B_0^2$ as a function of time. The middle and bottom panels show gray scale plots of the fluctuating magnetic field δB as a function of time and the wave vector k and as a function of time and the propagation angle θ_{kB} , respectively. Figure 2 shows that in the weakly collisional plasma the oblique

† The oblique fire hose has a lower threshold compared to that of the parallel fire hose at least up to $\beta_{p\parallel} = 10^4$; however, the two thresholds approach each other in the $(\beta_{p\parallel}, T_{p\perp}/T_{p\parallel})$ plane as $\beta_{p\parallel}$ increases.

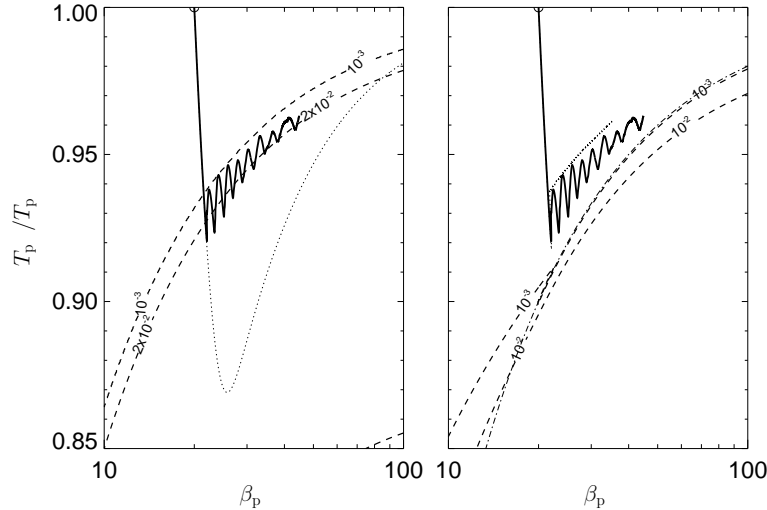


FIGURE 1. Solid curves denote the path in the $(\beta_{p\parallel}, T_{p\perp}/T_{p\parallel})$ space in the 2-D (fire hose) CHEB simulation. The dashed contours show the linear prediction, the maximum linear growth rate (in units of ω_{cp}) as a function of $\beta_{p\parallel}$ and $T_{p\perp}/T_{p\parallel}$ for (left) the oblique fire hose and (right) for the parallel fire hose. The dotted line on the left panel shows the theoretical collisional evolution, Eq. (3.2) whereas on the right panel it shows the theoretical prediction for a simple, one-mode quasi-linear model. The dash-dotted line displays the fluid fire hose threshold $C_F = 0$.

fire hose has an evolution similar to that of the collisionless case (Hellinger & Trávníček 2008). The oblique fire hose generates waves at oblique angles with respect to the ambient magnetic field. The spectrum evolves towards less oblique angles and most of the fluctuating energy is damped. The system with a low wave activity evolves roughly following the weakly collisional prediction till enough oblique fire hose wave energy is again generated and reduces the proton temperature anisotropy. This behavior continues in a semiperiodic manner with a period which seems to increase with time. On average the magnetic fluctuating energy increases with time, after each period there is more remaining fluctuating magnetic energy.

The linear and quasi-linear analyses (Hellinger & Matsumoto 2000, 2001) indicate that this behavior may be understood in the quasi-linear framework where a dispersion change is included. The oblique fire hose instability generates non-propagating modes which only exist for sufficiently anisotropic protons. As the generated waves scatter protons and reduce the proton anisotropy the non-propagating modes no longer exist and the corresponding wave energy must be transformed mainly to standard, ion cyclotron waves. These waves are relatively strongly damped by protons through the cyclotron resonance. In the collisionless plasmas this leads to a deformation of the proton VDFs in the resonant regions (Matteini *et al.* 2006; Hellinger & Trávníček 2008). This deformation is not seen in the present simulation as the Coulomb collisions are relatively strong (and the resonant interaction in the high beta plasma may be less obvious or possibly less effective, cf., Matteini *et al.* 2006). The proton VDFs (averaged over the box) remains relatively close to bi-Maxwellian ones during the simulation, so that the two parallel and perpendicular temperatures characterize very well the proton VDFs. This justifies the usage of the bi-Maxwellian Langevin model and, similarly, this may justify the application of the quasi-linear heating rates based on the bi-Maxwellian VDFs for the macroscopic description of the oblique fire hose instability; the one-mode model used here is, however, too simple

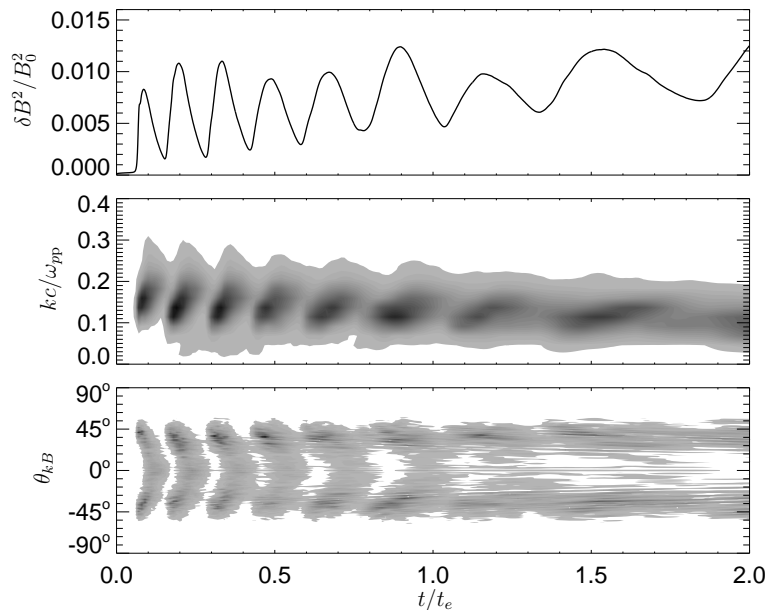


FIGURE 2. Evolution of the magnetic fluctuations in the 2-D (fire hose) CHEB simulation: (top) Fluctuating magnetic field $\delta B^2/B_0^2$ as a function of time. Gray scale plots of the fluctuating magnetic field δB as a function of time and k (middle panel) and as a function of time and θ_{kB} (bottom panel).

to capture the evolution of the system since it does not include the branch change from nonpropagating to propagating modes.

3.2. Mirror and ion cyclotron instabilities

In the second (mirror), 2-D CHEB simulation we initialize protons with isotropic bi-Maxwellian velocity distribution function with $\beta_p = 30$. In this case we impose a continuous expansion in the x and y directions with the (initial) characteristic expansion time $t_e = 10^4/\omega_{cp0}$ (the radial direction in the model of expanding solar wind would be in the z direction, i.e., perpendicular to \mathbf{B}_0 which is aligned with the x axis). The expansion leads to a decrease of the density as $(1 + t/t_e)^{-2}$ whereas the magnitude of the magnetic field decreases as $(1 + t/t_e)^{-1}$. In this case the double adiabatic evolution would lead to increasing $T_{p\perp}/T_{p\parallel}$. The collisional isotropization frequency ν_{pp} is chosen to be $6.5 \times 10^{-4}\omega_{cp}$.

Figure 3 shows the evolution of the system in the 2-D (mirror) CHEB simulation. Solid curves denote the path in the $(\beta_{p\parallel}, T_{p\perp}/T_{p\parallel})$ on both the panels ($\beta_{p\parallel}$ are $T_{p\perp}/T_{p\parallel}$ averaged over the box as in Figure 1). The dashed contours show the linear prediction, the maximum linear growth rate (in units of ω_{cp}) as a function of $\beta_{p\parallel}$ and $T_{p\perp}/T_{p\parallel}$ for the mirror instability (left panel) and for the ion (proton) cyclotron instability (right panel). The dotted line on the left panel shows the theoretical collisional evolution (given by Eq. (3.2)) whereas the dash-dotted line displays the mirror threshold $C_M = 0$ (cf., Chandrasekhar *et al.* 1958; Hellinger 2007) where

$$C_M = \beta_{p\perp}(T_{p\perp}/T_{p\parallel} - 1) - 1 - \frac{1}{2} \frac{(T_{p\perp}/T_{p\parallel} - 1)^2}{\beta_e^{-1} + \beta_{p\parallel}^{-1}}. \quad (3.5)$$

Figure 3 shows that the system initially follows the theoretical collisional prediction of Eq. (3.2). Again, the initial behavior of the system is almost double adiabatic but

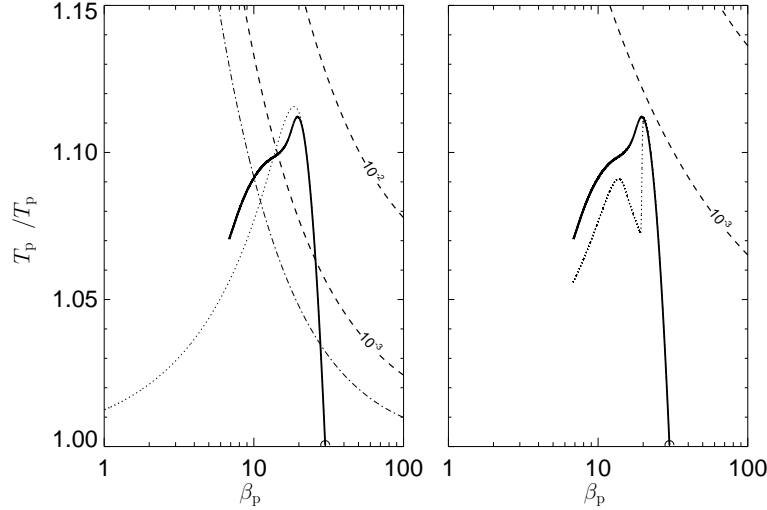


FIGURE 3. Solid curves denote the path in the $(\beta_{p\parallel}, T_{p\perp}/T_{p\parallel})$ space in the 2-D (mirror) CHEB simulation. The dashed contours show the linear prediction, the maximum linear growth rate (in units of ω_{cp}) as a function of $\beta_{p\parallel}$ and $T_{p\perp}/T_{p\parallel}$ for (left) mirror instability and (right) for the ion cyclotron instability. The dotted line on the left panel shows the theoretical collisional evolution, Eq. (3.2), whereas on the right panel it shows the theoretical prediction for a simple, one-mode quasi-linear model. The dash-dotted line displays the mirror threshold $C_M = 0$.

as the temperature anisotropy increases the system departs from the double adiabatic expectation, and, eventually, the collisional term would dominate and the system would asymptotically reach the isotropy. In the region unstable with respect to the mirror instability (in the corresponding collisionless plasma) the temperature anisotropy is reduced faster compared to the collisional prediction due to the generation of (mostly) mirror modes. This reduction continues in a manner qualitatively similar to the theoretical prediction likely mainly due to the Coulomb collisions. The dotted line on the right panel of Figure 3 shows a prediction of the simple one-mode quasi-linear model. It captures some of the properties of the simulated system, namely the fast reduction of the anisotropy. This model also exhibits an evolution following a marginal stability path with respect to the mirror instability.

The temporal evolution of the wave spectrum is shown in Figure 4: The top panel displays the fluctuating magnetic field $\delta B^2/B_0^2$, the middle and bottom panels show gray scale plots of the fluctuating magnetic field δB as a function of time and the wave vector k and as a function of time and the propagation angle θ_{kB} , respectively. The dash-dotted lines display the times when the system crosses the mirror threshold $C_M = 0$ (see Figure 3). Figure 4 shows that the fluctuating magnetic energy is generated later on in the simulation when the system is in the unstable region and this energy is then damped; at the end the system is in a region stable with respect to the mirror instability. The generated modes are at mostly strongly oblique angles which correspond to the mirror modes. There also weak signatures of quasi-parallel waves which correspond to the proton cyclotron modes.

The mirror modes remain in the system for a relatively long time even in the region linearly stable with respect to the mirror instability. This is likely related with the non-linear properties (bistability) of the mirror modes. The mirror instability tends to create coherent structures either in the form of magnetic enhancements (humps) or in the form of magnetic depressions (holes). The nonlinear model of Kuznetsov *et al.* (2007b,a) for

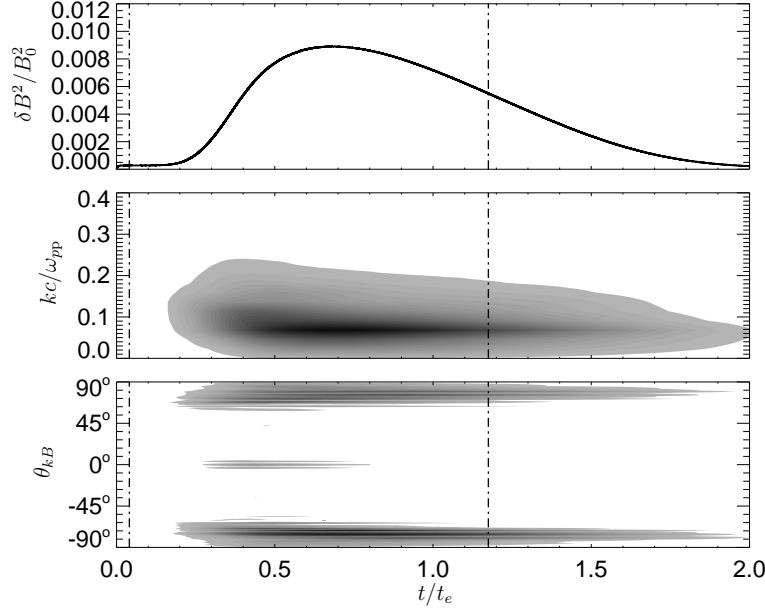


FIGURE 4. Evolution of the magnetic fluctuations in the 2-D mirror CHEB simulation: (top) Fluctuating magnetic field $\delta B^2/B_0^2$ as a function of time. Gray scale plots of the fluctuating magnetic field δB as a function of time and k (middle panel) and as a function of time and θ_{kB} (bottom panel). The dash-dotted lines display the time when the system crosses the mirror threshold $C_M = 0$.

nonlinear development of the mirror instability, near threshold based on a reductive perturbative expansion of Vlasov-Maxwell equations predicts formation of magnetic holes; however, numerical simulations exhibit rather formation of magnetic humps. This effect is likely connected with the resonant properties of the mirror instability. While the mirror modes near threshold appear at large scales, their driving mechanism is the Landau resonance between the nonpropagating mirror modes and protons with small parallel velocities. Small changes of proton velocity distribution function in the resonant regions strongly influences the nonlinear term derived from the perturbative expansion. This may lead to the change of sign of the nonlinearity and to the formation of magnetic humps instead of holes (Hellinger *et al.* 2009).

In the present CHEB simulation we observe initially a formation of magnetic humps in the unstable region. These humps are transformed to magnetic holes as the system becomes linearly stable with respect to the mirror instability. This can be seen in Figure 5 which displays the (sample estimate of) skewness of the amplitude of the magnetic field $g_1(B)$ (calculated at a given time over the 512x512 grid points) as a function of the mirror linear criterion C_M . The skewness of a variable x with N points is defined as

$$g_1(x) = \frac{\sqrt{N(N-1)}}{N-2} \frac{\langle (x - \langle x \rangle)^3 \rangle}{\langle (x - \langle x \rangle)^2 \rangle^{3/2}}$$

where $\langle x \rangle = \sum_{i=1}^N x_i / N$ denotes averaging. The system starts in the stable region with a zero skewness. As the system moves to the unstable regions the mirror modes are generated and the skewness becomes positive which is a sign of magnetic humps. As the Coulomb collisions drives the system to the stable region the skewness becomes negative indicating magnetic holes. Similar evolution is also observed in collisionless

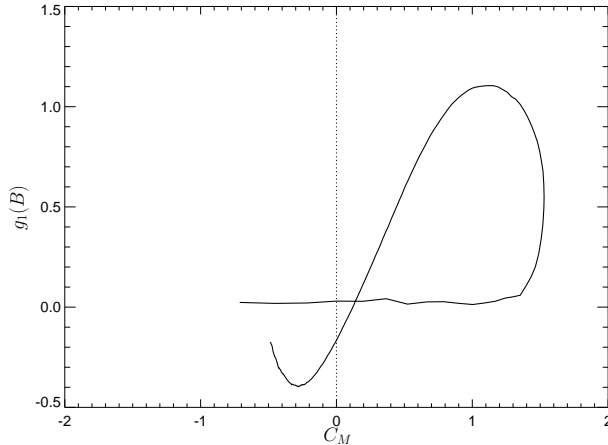


FIGURE 5. Evolution in the 2-D mirror CHEB code: Skewness of the amplitude of the magnetic field $g_1(B)$ as a function of the mirror linear criterion C_M .

hybrid expanding box simulations and there are signatures of a comparable trend in the terrestrial magnetosheath (Trávníček *et al.* 2007; Génot *et al.* 2009).

The proton velocity distribution function remains quite close to a bi-Maxwellian during the whole simulation as the Coulomb collisions are relatively strong. However, some weak signatures of flattening of the proton velocity distribution function in the resonant region are also observed (this is compatible with the presence of magnetic humps in the unstable region). Such a flattening is expected from the quasilinear predictions (Califano *et al.* 2008). The quasilinear approximation is, however, questionable when coherent structures appear; on the other hand, the proton trapping has a similar effect on the velocity distribution function (Porazik & Johnson 2013).

4. Discussion

In this paper we study evolution of expansion-driven temperature anisotropy in a weakly collisional, relatively high beta plasma using the CHEB model. We performed two 2D CHEB simulations, one for the fire hose instabilities and one for the mirror and ion cyclotron instabilities. The parameters for the two simulations were chosen as a compromise to have feasible runs in a kinetic particle-in-cell hybrid code; large betas lead to high numerical noise so that a large number of particles per cell is needed to have a good separation between the noise and waves generated by the instabilities. The inverse collisional frequency was chosen to be relatively large (but comparable) with respect to the expansion characteristic time. For the chosen parameters the expansion generates proton temperature anisotropies sufficient to destabilize the system despite the presence of relatively strong Coulomb collisions.

In the first CHEB simulation only the linearly dominant oblique fire hose is observed. The wave activity generated by this instability efficiently scatters protons and effectively reduces the proton temperature anisotropy (leading to an effective isotropization frequency much faster the collisional one). This instability has a self-stabilizing properties, most of the generated wave energy is reabsorbed by protons. The evolution exhibits an oscillation between unstable and marginally stable states with generation and absorption of the wave energy. In the second CHEB simulation we observed mainly the mirror mode activity. The mirror instability generates coherent structures in the form of magnetic humps which scatter protons. As the Coulomb collisions reduce the temperature

anisotropy the system becomes stable with respect to the mirror instability and the magnetic humps transform into magnetic holes which survive relatively long time in the stable region. We developed a simple, one-mode model based on quasi-linear heating rates for bi-Maxwellian velocity distribution functions. This model exhibit some basic properties of the two instabilities; a more general quasi-linear model may be useful for modeling of the macroscopic effects of the oblique fire hose instability and possibly of the mirror instability to some extent. More theoretical and numerical work is needed.

We used the expansion as a driver for the temperature anisotropy. In many astrophysical situations such as in the intracluster medium it is expected that a large scale (turbulent) motion leads to velocity shears which drive the temperature anisotropy. We expect that a similar evolution we observed in the case of expansion takes place also in the case of velocity shears. Indeed, recent (collisionless) hybrid shearing box simulations (Kunz *et al.* 2014) show similar properties. In the cases when the velocity shear generates $T_{p\perp} < T_{p\parallel}$ Kunz *et al.* (2014) observe oblique fire hose instability which efficiently reduces the temperature anisotropy. However, Kunz *et al.* (2014) don't observe oscillatory behavior comparable to our results. This is possibly due to the fact that Kunz *et al.* (2014) stop their simulations shortly after the fluctuating magnetic energy reaches the maximum. Moreover, our CHEB results indicate that the decaying time increases with the proton beta (and additional standard hybrid simulations of the oblique fire hose instability up to $\beta_{p\parallel} = 100$ confirm this trend) and Kunz *et al.* (2014) investigated cases with $\beta_{p\parallel} \sim 200$. In the cases when the velocity shear generates $T_{p\perp} > T_{p\parallel}$ Kunz *et al.* (2014) observe mirror mode structures which trap and scatter protons. This is similar to our results. We note, however, that in our case relatively strong Coulomb collisions are present and scatter protons which likely reduces proton trapping. This may possibly contribute to the quasi-linear diffusion.†

In our weakly collisional simulations the instabilities have nonlinear properties relatively similar to those in collisionless plasmas. In the case of oblique fire hose instability the nonlinear evolution which may be understood in the quasi-linear framework including a branch change. In this case the macroscopic properties may be partly described by a combination of collisional and quasi-linear terms. The case of the mirror instability is more complicated. The mirror instabilities generates nonlinear structure which evolve in time and survive relatively long into the stable region (introducing a memory in the system). The mirror structures reduce the anisotropy by scattering protons which can be only partially described as a quasi-linear diffusion. In our CHEB simulations (as well as in simulations using the shearing box model) the external driver is modeled as an independent force. Therefore, these models cannot be used to study the feedback of temperature-anisotropy-driven instabilities on the driver. For instance, general properties of the viscosity tensor remain an open problem (cf., Mogavero & Schekochihin 2014).

Acknowledgements

Authors acknowledge the grant P209/12/2023 of the Grant Agency of the Czech Republic. The research leading to these results has received funding from the European Commission's Seventh Framework Programme (FP7) under the grant agreement SHOCK (project number 284515, project-shock.eu). This work was also supported by the projects RVO:67985815 and RVO:68378289.

† Particle trapping and quasi-linear diffusion are two connected phenomena. A quasi-linear-like diffusion appears when the trapped regions for different noncoherent modes sufficiently overlaps (Chirikov 1979).

REFERENCES

- BALE, S. D., KASPER, J. C., HOWES, G. G., QUATAERT, E., SALEM, C. & SUNDKVIST, D. 2009 Magnetic fluctuation power near proton temperature anisotropy instability thresholds in the solar wind. *Phys. Rev. Lett.* **103**, 211101.
- BARAKAT, A. R. & SCHUNK, R. W. 1981 Momentum and energy exchange collision terms for interpenetrating bi-Maxwellian gases. *J. Phys. D: Appl. Phys.* **14**, 421–438.
- BRAGINSKII, S. I. 1965 Transport processes in a plasma. In *Rev. Plasma Phys.* (ed. M. Leontovich), vol. 1, p. 205. New York: Consultants Bureau.
- CALIFANO, F., HELLINGER, P., KUZNETSOV, E., PASSOT, T., SULEM, P.-L. & TRÁVNÍČEK, P. M. 2008 Nonlinear mirror mode dynamics: Simulations and modeling. *J. Geophys. Res.* **113**, A08219.
- CHANDRAN, B. D. G., DENNIS, T. J., QUATAERT, E. & BALE, S. D. 2011 Incorporating kinetic physics into a two-fluid solar-wind model with temperature anisotropy and low-frequency Alfvén-wave turbulence. *Astrophys. J.* **743**, 197.
- CHANDRASEKHAR, S. A., KAUFMAN, A. N. & WATSON, K. M. 1958 The stability of the pinch. *Proc. R. Soc. London, Ser. A* **245**, 435.
- CHEW, G. F., GOLDBERGER, M. L. & LOW, F. E. 1956 The Boltzmann equation and the one fluid hydromagnetic equations in the absence of particle collisions. *Proc. R. Soc. London* **A236**, 112–118.
- CHIRIKOV, B. V. 1979 A universal instability of many-dimensional oscillator systems. *Phys. Rep.* **52**, 263–379.
- DENTON, R. E., ANDERSON, B. J., GARY, S. P. & FUSELIER, S. A. 1994 Bounded anisotropy fluid model for ion temperatures. *J. Geophys. Res.* **99**, 11225–11241.
- GARY, S. P. 1993 *Theory of Space Plasma Microinstabilities*. New York: Cambridge Univ. Press.
- GÉNOT, V., BUDNIK, E., HELLINGER, P., PASSOT, T., BELMONT, G., TRÁVNÍČEK, P. M., SULEM, P. L., LUCEK, E. & DANDOURAS, I. 2009 Mirror structures above and below the linear instability threshold: Cluster observations, fluid model and hybrid simulations. *Ann. Geophys.* **27**, 601–615.
- GRAPPIN, R., VELLI, M. & MANGENEY, A. 1993 Nonlinear-wave evolution in the expanding solar wind. *Phys. Rev. Lett.* **70**, 2190–2193.
- HASEGAWA, A. 1969 Drift mirror instability in the magnetosphere. *Phys. Fluids* **12**, 2642–2650.
- HELLINGER, P. 2007 Comment on the linear mirror instability near the threshold. *Phys. Plasmas* **14**, 082105.
- HELLINGER, P., KUZNETSOV, E. A., PASSOT, T., SULEM, P. L. & TRÁVNÍČEK, P. M. 2009 Mirror instability: From quasi-linear diffusion to coherent structures. *Geophys. Res. Lett.* **36**, L06103.
- HELLINGER, P. & MATSUMOTO, H. 2000 New kinetic instability: Oblique Alfvén fire hose. *J. Geophys. Res.* **105**, 10519–10526.
- HELLINGER, P. & MATSUMOTO, H. 2001 Nonlinear competition between the whistler and Alfvén fire hoses. *J. Geophys. Res.* **106**, 13215–13218.
- HELLINGER, P., PASSOT, T., SULEM, P.-L. & TRÁVNÍČEK, P. M. 2013 Quasi-linear heating and acceleration in bi-Maxwellian plasmas. *Phys. Plasmas* **20**, 122306.
- HELLINGER, P. & TRÁVNÍČEK, P. 2005 Magnetosheath compression: Role of characteristic compression time, alpha particle abundances and alpha/proton relative velocity. *J. Geophys. Res.* **110**, A04210.
- HELLINGER, P. & TRÁVNÍČEK, P. M. 2008 Oblique proton fire hose instability in the expanding solar wind: Hybrid simulations. *J. Geophys. Res.* **113**, A10109.
- HELLINGER, P., TRÁVNÍČEK, P., KASPER, J. C. & LAZARUS, A. J. 2006 Solar wind proton temperature anisotropy: Linear theory and WIND/SWE observations. *Geophys. Res. Lett.* **33**, L09101.
- HELLINGER, P. & TRÁVNÍČEK, P. M. 2009 On Coulomb collisions in bi-Maxwellian plasmas. *Phys. Plasmas* **16**, 054501.
- HELLINGER, P. & TRÁVNÍČEK, P. M. 2010 Langevin representation of Coulomb collisions for bi-Maxwellian plasmas. *J. Comput. Phys.* **229**, 5432–5439.
- HELLINGER, P. & TRÁVNÍČEK, P. M. 2012 On the quasi-linear diffusion in collisionless plasmas (to say nothing about Landau damping). *Phys. Plasmas* **19**, 062307.

- HELLINGER, P. & TRÁVNÍČEK, P. M. 2014 Solar wind protons at 1 AU: Trends and bounds, constraints and correlations. *Astrophys. J. Lett.* **784**, L15.
- KENNEL, C. F. & ENGELMANN, F. 1966 Velocity space diffusion from weak plasma turbulence in a magnetic field. *Phys. Fluids* **9**, 2377–2388.
- KUNZ, M. W., SCHEKOCHIHIN, A. A. & STONE, J. M. 2014 Firehose and mirror instabilities in a collisionless shearing plasma. *Phys. Rev. Lett.* **112**, 205003.
- KUZNETSOV, E. A., PASSOT, T. & SULEM, P.-L. 2007a Nonlinear theory of mirror instability near threshold. *JETP Lett.* **86**, 637–642.
- KUZNETSOV, E. A., PASSOT, T. & SULEM, P.-L. 2007b Dynamical model for nonlinear mirror modes near threshold. *Phys. Rev. Lett.* **98**, 235003.
- MANHEIMER, W. M., LAMPE, M. & JOYCE, G. 1997 Langevin representation of Coulomb collisions in PIC simulations. *J. Comput. Phys.* **138**, 563–584.
- MATTEINI, L., LANDI, S., HELLINGER, P. & VELLI, M. 2006 Parallel proton fire hose instability in the expanding solar wind: Hybrid simulations. *J. Geophys. Res.* **111**, A10101.
- MATTHEWS, A. 1994 Current advance method and cyclic leapfrog for 2D multispecies hybrid plasma simulations. *J. Comput. Phys.* **112**, 102–116.
- MOGAVERO, F. & SCHEKOCHIHIN, A. A. 2014 Models of magnetic field evolution and effective viscosity in weakly collisional extragalactic plasmas. *Mon. Not. R. Astron. Soc.* **440**, 3226–3242.
- PORAZIK, P. & JOHNSON, J. R. 2013 Gyrokinetic particle simulation of nonlinear evolution of mirror instability. *J. Geophys. Res.* **118**, 7211–7218.
- ROSIN, M. S., SCHEKOCHIHIN, A. A., RINCON, F. & COWLEY, S. C. 2011 A nonlinear theory of the parallel firehose and gyrothermal instabilities in a weakly collisional plasma. *Mon. Not. R. Astron. Soc.* **413**, 7–38.
- SANTOS-LIMA, R., DE GOUVEIA DAL PINO, E. M., KOWAL, G., FALCETA-GONÇALVES, D., LAZARIAN, A. & NAKWACKI, M. S. 2014 Magnetic field amplification and evolution in turbulent collisionless magnetohydrodynamics: An application to the intracluster medium. *Astrophys. J.* **781**, 84.
- SCHEKOCHIHIN, A. A., COWLEY, S. C., DORLAND, W., HAMMETT, G. W., HOWES, G. G., PLUNK, G. G., QUATAERT, E. & TATSUNO, T. 2008 Gyrokinetic turbulence: a nonlinear route to dissipation through phase space. *Plasma Phys. Control. Fusion* **50**, 124024.
- SHOUB, E. C. 1987 Failure of the Fokker-Planck approximation to the Boltzmann integral for $(1/r)$ potentials. *Phys. Fluids* **30**, 1340–1352.
- TRÁVNÍČEK, P., HELLINGER, P., TAYLOR, M. G. G. T., ESCOUBET, C. P., DANDOURAS, I. & LUCEK, E. 2007 Magnetosheath plasma expansion: Hybrid simulations. *Geophys. Res. Lett.* **34**, L15104.
- WICKS, R. T., MATTEINI, L., HORBURY, T. S., HELLINGER, P. & ROBERTS, A. D. 2013 Temperature anisotropy instabilities; combining plasma and magnetic field data at different distances from the sun. In *Proc. 13th Int. Solar Wind Conf.*, , vol. 1539, pp. 303–306. AIP.
- YOON, P. H. & SEOUGH, J. 2012 Quasilinear theory of anisotropy-beta relation for combined mirror and proton cyclotron instabilities. *J. Geophys. Res.* **117**, A08102.